geosciences

MDPI

Article

Statistical Analysis of Mt. Vesuvius Earthquakes Highlights Pitfalls in Magnitude Estimation

Cataldo Godano [1,2,†] and Nicola Alessandro Pino [2,*,†]

1 Dipartimento di Matematica e Fisica, Università della Campania "Luigi Vanvitelli", 81100 Caserta, Italy; cataldo.godano@unicampania.it
2 Istituto Nazionale di Geofisica e Vulcanologia, Sezione di Napoli, 80124 Napoli, Italy
* Correspondence: alessandro.pino@ingv.it
† These authors contributed equally to this work.

Abstract: Here, we characterize the statistical behaviour of the Mt. Vesuvius seismicity using distinct available catalogues. Our analysis confirms that for this area, the GR distribution exhibited two scaling regimes of the *b*-value, not commonly observed for the standard frequency-magnitude distribution of earthquakes. By assuming a physical cause, we tested four different hypotheses for the source of the break in the scaling: finite size effect, depth variations in the *b*-value, radial dependence in the *b*-value, and different *b*-values for swarm and non-swarm events. None of the above reasons are able to explain the observation. Thus, we investigated the possibility of some pitfalls in magnitude estimation. Based on our analysis, we suggest there is a bias in the duration magnitude the catalogues are based on. This is due to the arbitrary extrapolation to smaller magnitudes of a linear regression derived for earthquakes with $m \geq 3.0$. When a suitable correction is applied to the estimated magnitude, the GR distribution assumes the usual shape, with a *b*-value closer to that usually observed in volcanic areas. Finally, the analysis of the time variation of some statistical parameters reveals that the state of the volcano appears to be stationary over the entire analysed period, possibly with only a slight decrease in the *b*-value, indicating a small reduction in differential stress.

Keywords: Gutenberg–Richter (GR) distribution; estimating b and m_c values; double scaling in the GR distribution

check for updates

Citation: Godano, C.; Pino, N.A. Statistical Analysis of Mt. Vesuvius Earthquakes Highlights Pitfalls in Magnitude Estimation. *Geosciences* **2024**, *14*, 15. https://doi.org/10.3390/geosciences14010015

Academic Editors: Jesus Martinez-Frias and Luciano Telesca

Received: 29 November 2023
Revised: 29 December 2023
Accepted: 30 December 2023
Published: 3 January 2024

1. Introduction

Mt. Vesuvius is a composite strato-volcano located in the Campania Plain (Southern Italy), belonging to the Somma–Vesuvius volcanic complex. It is 1281 m high and 10 km wide. Some eruptive fissures, aligned in the E–W and N–S directions, cross the Mt. Somma caldera and the southern and western flanks of Vesuvius [1]. A melted zone has been individuated at ∼8 km depth [2,3], whereas the presence of a deep reservoir at depths of about 2.5–5.0 km b.s.l. has been hypothesized by Chiodini et al. [4], Del Pezzo et al. [5].

The seismicity of Mt. Vesuvius is characterized by low energy earthquakes, mainly distributed around the crater axis, at depths between 0 and 1 km (Figure 1). The strongest event since the end of the last eruption in 1944 occurred on 9 October 1999, with a magnitude of m_d = 3.6 [6]. The regional tectonic stress and the gravitational load—in association with both the hydrothermal activity in the crater area and episodes of injection of deeper magmatic fluids—should be at the basis of the local seismicity [4,7].

The b parameter of the Gutenberg–Richter (GR) distribution [8] represents one of the most important parameters in the characterization of seismic occurrence because (i) it is crucial in the evaluation of the seismic hazard and (ii) it is inversely correlated to the stress state [9–12].

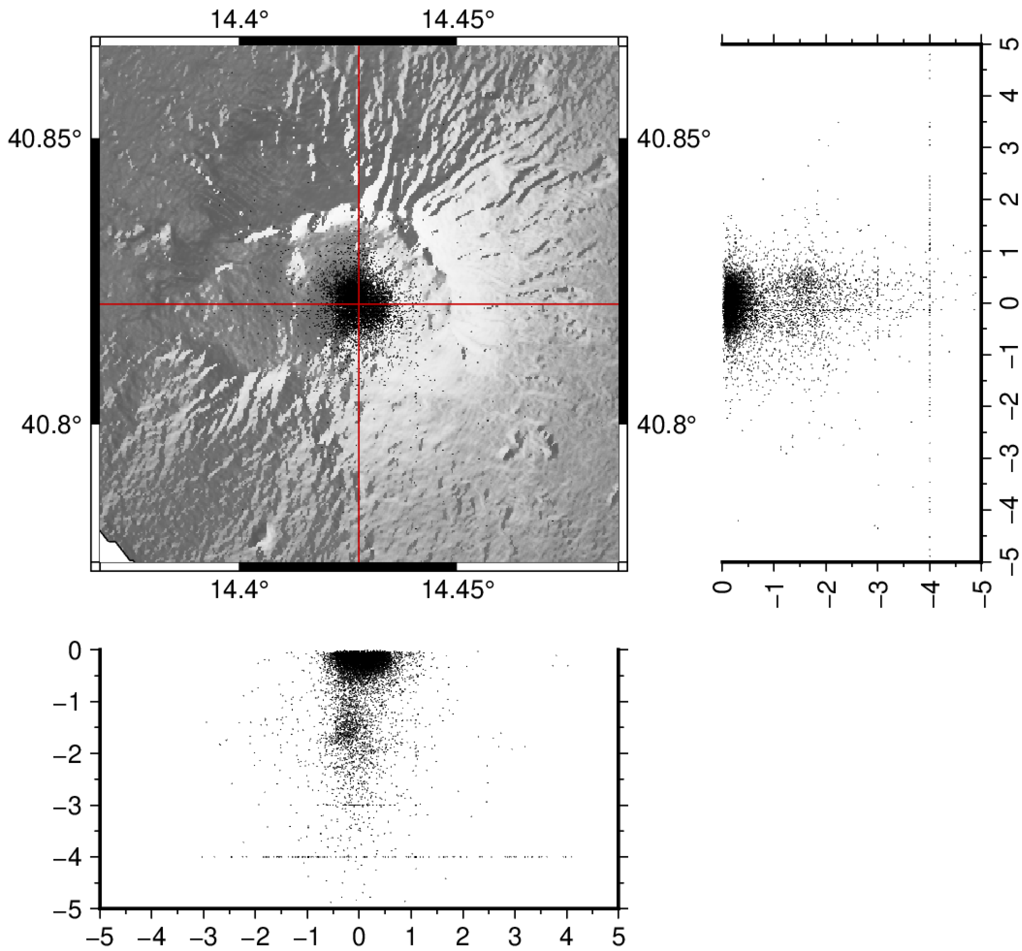

Figure 1. Map of Mt. Vesuvius displaying the located earthquakes for 1999–2023. Data are from the Seismolab Catalogue of INGV-Osservatorio Vesuviano, (https://www.ov.ingv.it, accessed on 28 November 2023). The lower (right) panel displays the earthquakes' projection on the N–S (W–E) vertical profile, whose surface trace is indicated in red in the map.

The spatial distribution of the *b*-value has been largely used to characterize stress regimes [13] and the spatial variations of the stress intensity in different seismogenic areas [14–16], including intermediate and deep seismic zones [17]. Several studies have also investigated the distribution of the *b*-value to individuate asperities on active faults [14,15,18], to characterize the complexity of the fault geometry [19], or to discriminate between distributed and on-fault seismicity [20]. Its analysis can also help in enlightening the presence of magmatic chambers in volcanic areas [15,21–23].

The time variations in the *b*-value represent a useful instrument for characterizing the nature of earthquakes in seismic sequences. Indeed, the variation in the *b*-value with time has been investigated to highlight the differences between foreshocks and background seismic activity [24–29] or to predictively discriminate between large foreshocks and mainshock [30]. Also, by stacking many earthquake sequences, an increase in *b*-value has been observed right after the occurrence of a mainshock [31].

Differently from tectonic earthquakes, quite often, volcanic events cluster in space and time without a triggering event of a higher magnitude [32]. These kinds of seismic sequences are called swarms. In general, they are recorded in either volcanic or geothermal areas, or even in tectonic environments [33–35]. It has been suggested that swarms occur in regions characterized by a high heterogeneity in terms of their material properties and stress concentration [36]. Their activity has been associated with stress changes induced by aseismic processes such as pore pressure changes [37] or fluid intrusion [35,38–41]. Volcanic swarms are usually the main reported seismic precursor for volcanic eruptions, especially for volcanoes that have been silent for decades or longer [33]. Although many models have modified the original ETAS model [42,43] and been able to reproduce some statistical feature of the seismic swarms [44–47], they have not been able to fit the occurrence rate: neither the Omori law [48] nor a simple relationship can describe the temporal evolution of the volcanic earthquake's swarms well. The reason for such a difficulty is the duration of the swarms, which are often very short and do not provide a sufficient number of events for a reliable statistical analysis. However, by stacking many swarms with an average rate of occurrence, an analytic expression that reproduces the experimental observations can be derived [49].

The inter-event time between two successive earthquakes, Δt, represents a powerful instrument to investigate the clustering properties of seismic events [50]. The Δt distribution $p(\Delta t)$ can be considered universal when the inter-event times Δt are rescaled by the mean occurrence rate, R [51–54]. In other words, R defines a 'local' time scale that characterizes the earthquake occurrence, whereas their clustering properties can be considered universal. This result was firstly obtained for pseudo-stationary periods, revealing that earthquakes tend to cluster even if their occurrence is apparently Poissonian [52]. The universality of $p(\Delta t)$ has also been observed for non-stationary periods [55] and for aftershock sequences [56,57]. Although the universal behaviour of $p(\Delta t)$ has been questioned [58–64], the departure from universality, observed at small Δt, has been explained in terms of four typical time scales [65]: the inverse rate of independent events, λ; the mean inverse rate of correlated events; the time parameter c defined in the Omori law [48]; and the catalogue duration T (this latter is irrelevant for the analysis presented here). A simpler approach defines a new expression for $p(\Delta t)$, including the departure from universality [66]. Exception to this behaviour is observed for volcanic explosion-quakes (i.e., Stromboli), which may exhibit a Poissonian behaviour [67] that can be explained in terms of bubble formation in the magma chamber.

Here, we analyse the seismicity of mount Vesuvius, evidencing some peculiar behaviour of the Gutenberg–Richter (GR) distribution.

2. Data: The Catalogues of the Mt. Vesuvius Instrumental Seismicity

Although the settlement of the Vesuvius Observatory (National Institute of Geophysics and Volcanology; INGV-OV) dates back to 1841 and the detection of local seismicity has been carried out since the first seismic detector was installed by [68], a regular collection of data relative to the occurrence of earthquakes has not been preserved up until about the half of the last century (e.g., [69–71]). However, because of discontinuity in both the number and type of the installed instruments, the data cannot be considered homogeneous, at least for some further decades.

At present, three catalogues of the Mt. Vesuvius instrumental seismicity are available for previous decades, starting in different years (Table 1). Two of these were based on single-station detection and magnitude estimation (OVO, BKE; Figure 2), these databases [72,73] cover up to 2021 and, according to the authors, they will be updated periodically, supposedly for historical continuity. The third one (ALL) is the current ordinary catalogue. It relies on the recordings of the monitoring seismic network, run by INGV-OV, and is regularly compiled according to modern standards.

Table 1. Mt. Vesuvius instrumental seismicity catalogues. Only events with an assigned magnitude are considered.

Catalogue	Starting Time	Ending Time	No. of Earthquakes
OVO	23 February 1972	27 December 2021	11,679
BKE	1 January 1999	31 December 2021	19,096
ALL	1 January 1999	8 September 2023	20,615
LOC	1 January 1999	8 September 2023	8766

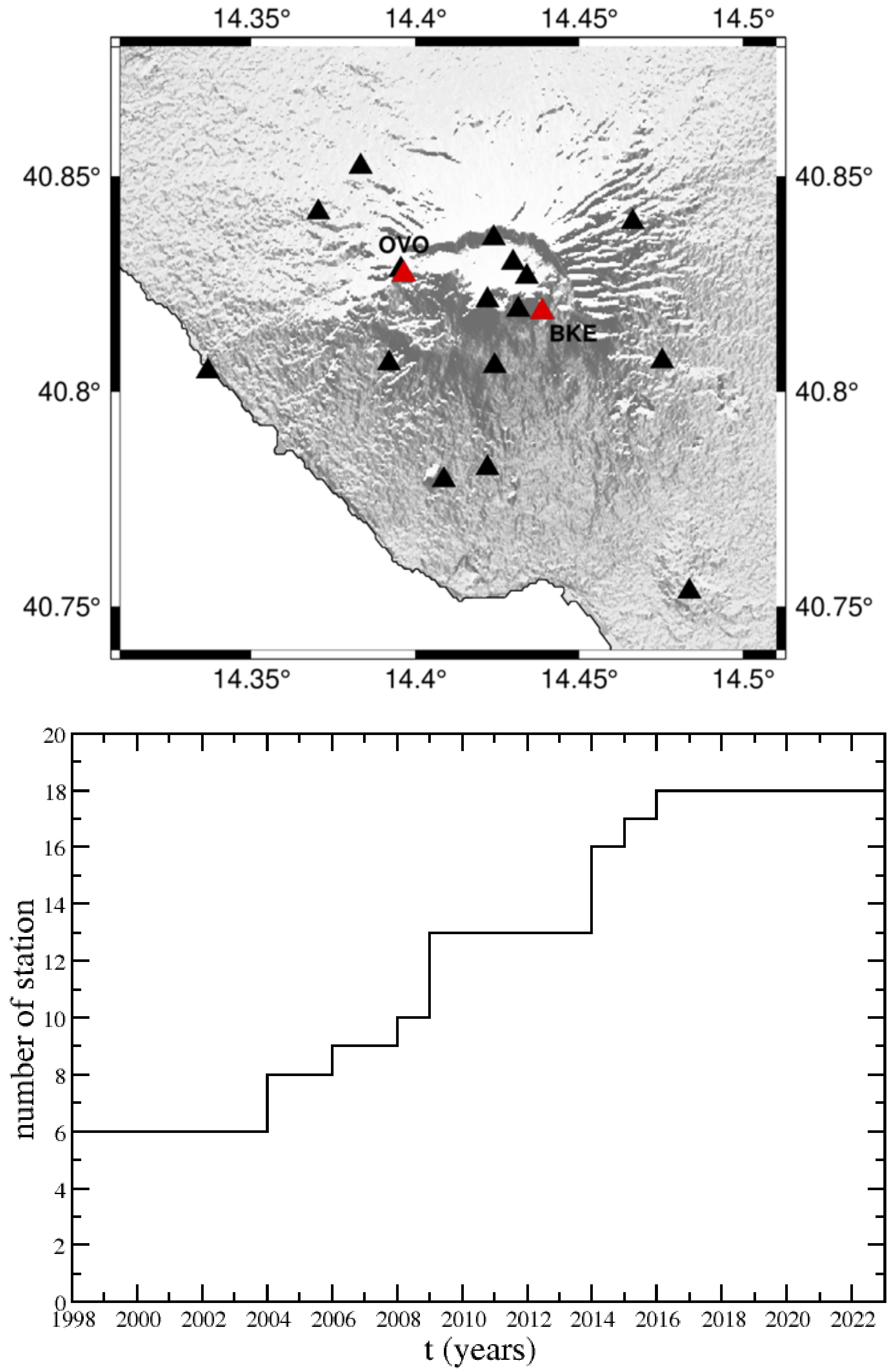

Figure 2. Upper panel: map of the present Mt. Vesuvius seismic monitoring network, run by INGV-OV. The red triangles indicate the stations OVO and BKE, historically used as reference for compiling respective single-station catalogues of the instrumental seismicity. The sites are equipped with either a short period or a broadband seismometer. Lower panel: number of stations composing the seismic network, since 1998.

The OVO and BKE catalogues cover the periods 1972–2021 and 1999–2021 (Figure 3), respectively. For both databases, each record contains the date, origin time, and event magnitude. The latter is only available as the duration magnitude m_d, which is the only one usually estimated at INGV-Osservatorio Vesuviano. The m_d at OVO is determined from the coda duration, τ, and is evaluated manually by the operator and converted according to the formula:

$$m_{d_{OVO}} = 2.75 \log \tau - 2.35. \tag{1}$$

This equation was derived by analysing regional earthquakes and comparing the waveform duration observed at OVO with the local magnitude m_L for the same event, as determined from the recording of the Wood–Anderson seismometer installed at Roma Monte Porzio (RMP), about 180 km apart [74]. Because of the distance between the two stations, the comparison was limited to events with $m \geq 3.0$, then extrapolated to lower magnitudes. Later on, starting from this parent relation, an analogous relation was obtained for BKE by comparing the duration observed at this station with the one determined at OVO:

$$m_{d_{BKE}} = 2.75 \log(\tau^{1.2} \cdot 0.37) - 2.35. \tag{2}$$

This station, located in proximity of the crater axis, i.e., closer to where most earthquakes occur, was significantly more sensitive to the lower magnitude events. Indeed, where they overlap, the BKE catalogue included many more earthquakes with respect to OVO (Figure 3). As a consequence, this station was usually considered at INGV-OV to estimate m_d for earthquakes recorded at the local seismic network and this was the value reported in the ALL catalogue.

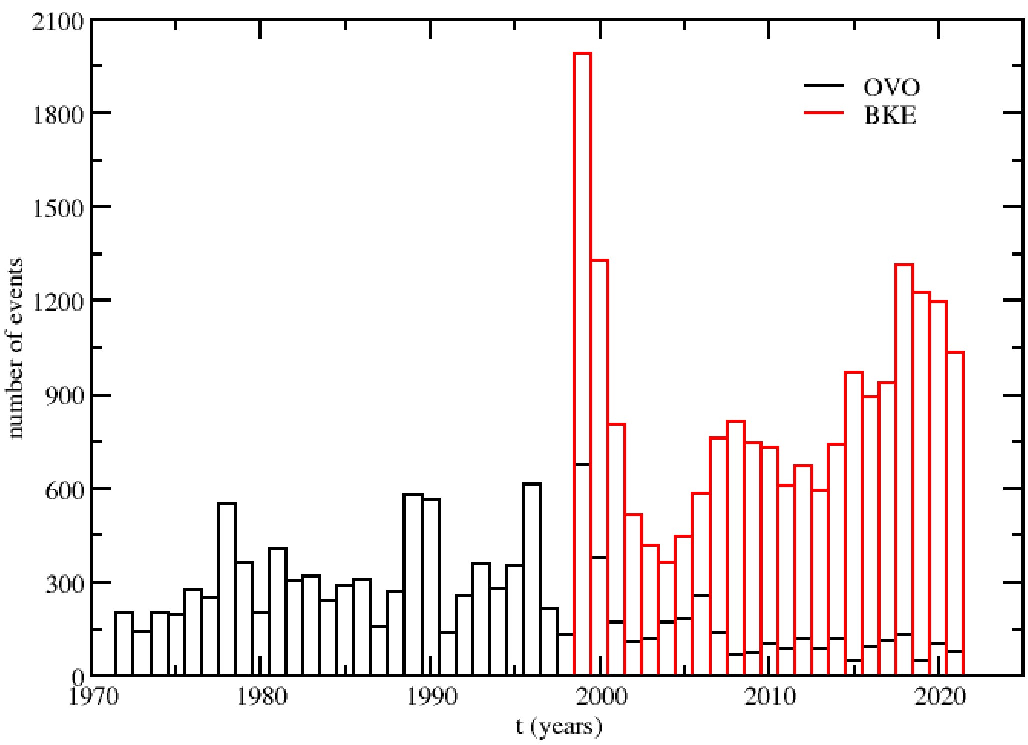

Figure 3. Histogram displaying the number of events/year of the OVO and the BKE catalogues.

Apart from the difference between these two catalogues, the number of events per year in the OVO catalogue significantly dropped after 2000, from an average of 318 earthquakes per year in 1972–2000 to 114 earthquakes per year in 2001–2021. In order to verify if this was a natural effect or if it was due to an oversight of the OVO catalogue, after the installation of the more sensitive BKE station in 1999, we compared the databases by excluding the earthquakes with $m < 2.0$ (Figure 4), a value reasonably above the magnitude of completeness for both, as determined by the following analysis (Section 3).

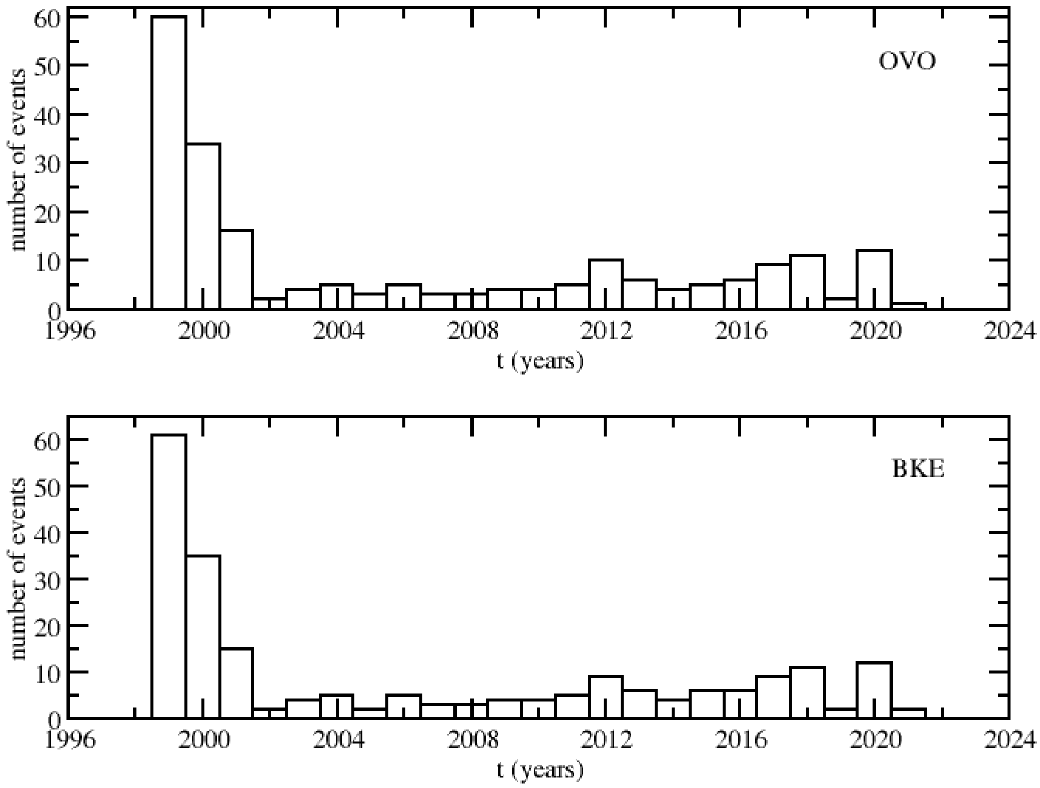

Figure 4. Histogram displaying the number of $m \geq 2.0$ events/year for the OVO and BKE catalogue, during 1999–2021.

The number of earthquakes per year in the two catalogues was very similar, differing by one at most, indicating that all of the local earthquakes with $m \geq 2.0$ for 1999–2021 were included in OVO; hence, this was likely to also be true for the preceding years. It follows that, rather than an artefact, the apparent decrease in the number of reported earthquakes after 2001 must have been a real effect, associated with reduced seismic activity within the volcanic structure. Thus, we used the whole catalogue for the statistical analyses. Besides these relatively long-standing instrumental earthquake catalogues, we also considered the ordinary, current catalogue (ALL; up to 9 October 2023), composed of earthquakes recorded from the whole monitoring network. It includes both located earthquakes and events for which no location could be determined. Thus, pointing to a full exploitation of the information, we also selected a subset of this database by extracting only the located earthquakes (LOC catalogue) and we analysed them separately. Because of the evolution of the network in the last 25 years (Figure 2), the number of located earthquakes increased significantly with time, in particular starting from 2015. This implied an improvement in the network sensitivity, with a decrease in the completeness magnitude.

3. The Gutenberg–Richter Distribution and the *b*-Value: Evidence for a Double Scaling

As a first step, we evaluated the completeness magnitude m_c of the whole catalogues.

Several methods have been proposed for estimating this parameter. For instance, commonly used techniques are (i) the maximum curvature technique [75], which fixes m_c at the magnitude value for which the maximum of the non cumulative GR distribution is observed; (ii) the goodness of fit [75], based on the exponential fit of the GR as a function of a threshold magnitude m_{th}, which selects m_c as the first m_{th} for which an accurate fit is obtained; (iii) the b-value stability approach [76], which chooses m_c as the magnitude threshold value at which the estimated b value becomes stable; (iv) the entire magnitude range method [77], which uses the entire range of magnitude and multiplies the GR distribution by a complementary error function; and (v) the harmonic mean method introduced by [78,79].

Here, we adopt the method based on the evaluation of the variability coefficient c_V, which is defined as the ratio between the standard deviation of the magnitude and its average value [80] with $c_V = 1$ for an exponential distribution. By evaluating its value as a function of a threshold magnitude m_{th}, it is possible to identify m_c as the m_{th} value, where c_V reached a provided value. Here, we fixed this threshold value at 0.93, which simulations with synthetic catalogues revealed to be the best choice for retrieving the correct m_c, while smaller and larger values tended to underestimate and overestimate m_c, respectively. Figure 5 shows c_V as a function of m_{th} for the four analysed catalogues. The results indicate $m_c = -0.2$ for the BKE and ALL catalogues and ~ 1.4 for OVO (Table 2). Conversely, for LOC, c_V overcomes the threshold value at $m_{th} \sim 1.8$, even though at ~ 0.0, it reaches a stable value. However, the break in the curve, with the exception of the OVO catalogue, reveals a more complex situation. Indeed, for three catalogues out of four, the GR distribution exhibited a two scaling pattern (Figure 6) confirming the results of [81]. As for OVO, we speculate that the higher m_c might have possibly hidden the double scaling, which was clearly visible instead when the seismic moment M_0 (thus a non-logarithmic scale) was considered (see below, Section 3.1).

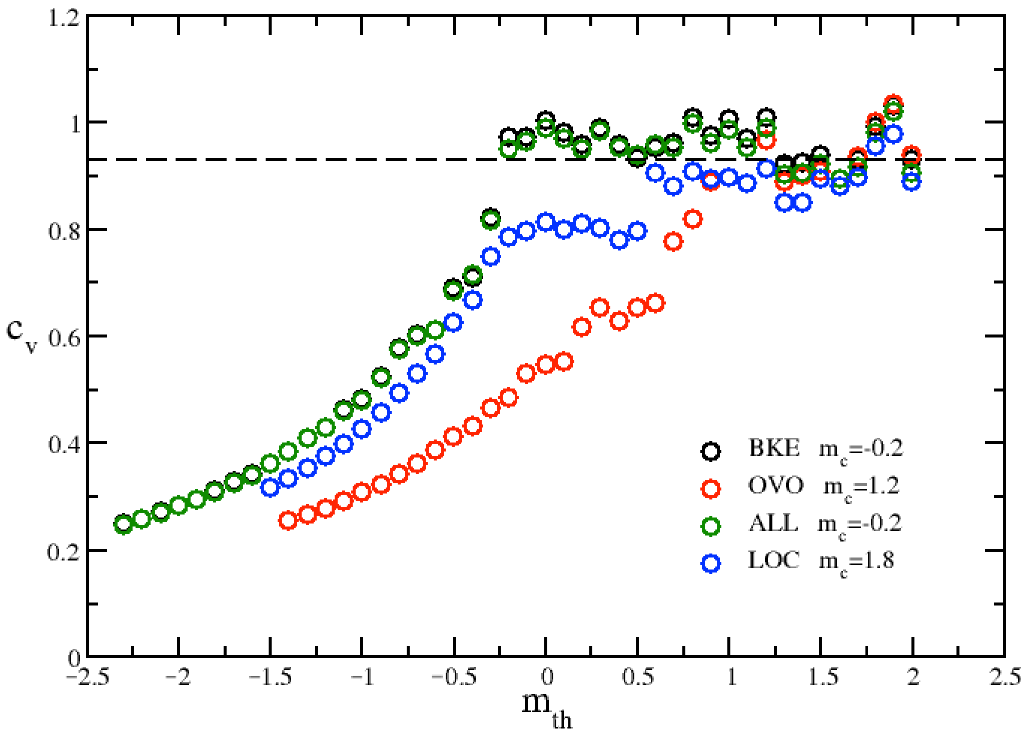

Figure 5. c_V vs. m_{th} for the four catalogues analysed here. The dashed black line represents the level $c_V = 0.93$.

Table 2. The completeness magnitudes, the *b*-values with their standard deviations, and the number of events N after the removal of the earthquakes with $m < m_c$.

Catalogue	m_c	b	σ_b	N
BKE	2.3	1.80	0.15	131
OVO	2.3	1.87	0.76×10^{-1}	548
ALL	2.3	1.86	0.75×10^{-1}	548
LOC	2.3	1.79	0.14	136
BKE	−0.2	0.75	0.52×10^{-2}	15,631
OVO	0.9	0.79	0.61×10^{-2}	7565
LOC	0.0	0.68	0.68×10^{-2}	6895
ALL	−0.2	0.76	0.55×10^{-2}	24,498

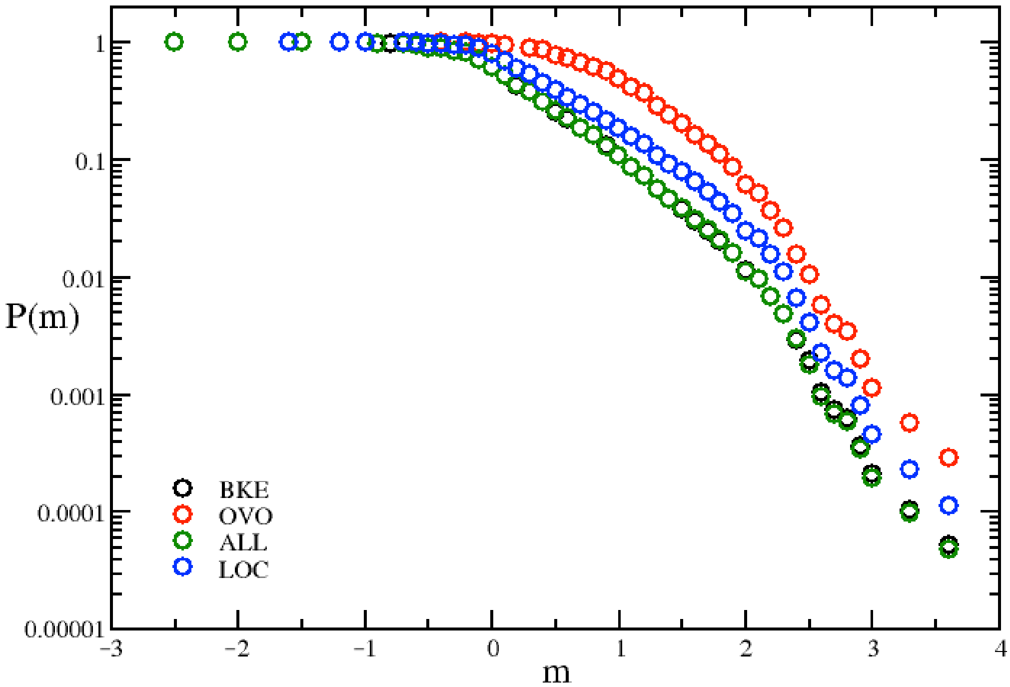

Figure 6. The GR distribution for the four catalogues analysed here.

It is worth noting that, as expected, the GR distributions for ALL and BKE appearred to be almost identical (Figure 6). This was derived from the high BKE sensitivity to the lower magnitude Mt. Vesuvius seismicity, resulting in practically all of the occurring local earthquakes being included in the BKE catalogue. Indeed, the difference was mostly due to the ∼1400 events occurring during 2022–2023, when they did not overlap.

To better display the existence of the two regimes in the GR distributions and to estimate the two m_c values, we evaluated c_V in narrower magnitude ranges with respect to what is shown in Figure 5. The first range went from −0.5 to 1.8 and the c_V evaluation confirmed $m_c = -0.2$ for the BKE and ALL catalogues (Figure 7). Conversely, OVO and LOC never reached the c_V threshold value of 0.93. However, the c_V value assumed an approximately constant value at $m_{th} = 0.9$ for OVO and at $m_{th} = 0$ for LOC. These values can be assumed to correspond to m_c for those catalogues. The analysis in the second range, from 1.7 to 2.5, revealed that $m_c = 2.2$ was true for all of the catalogues (Figure 8).

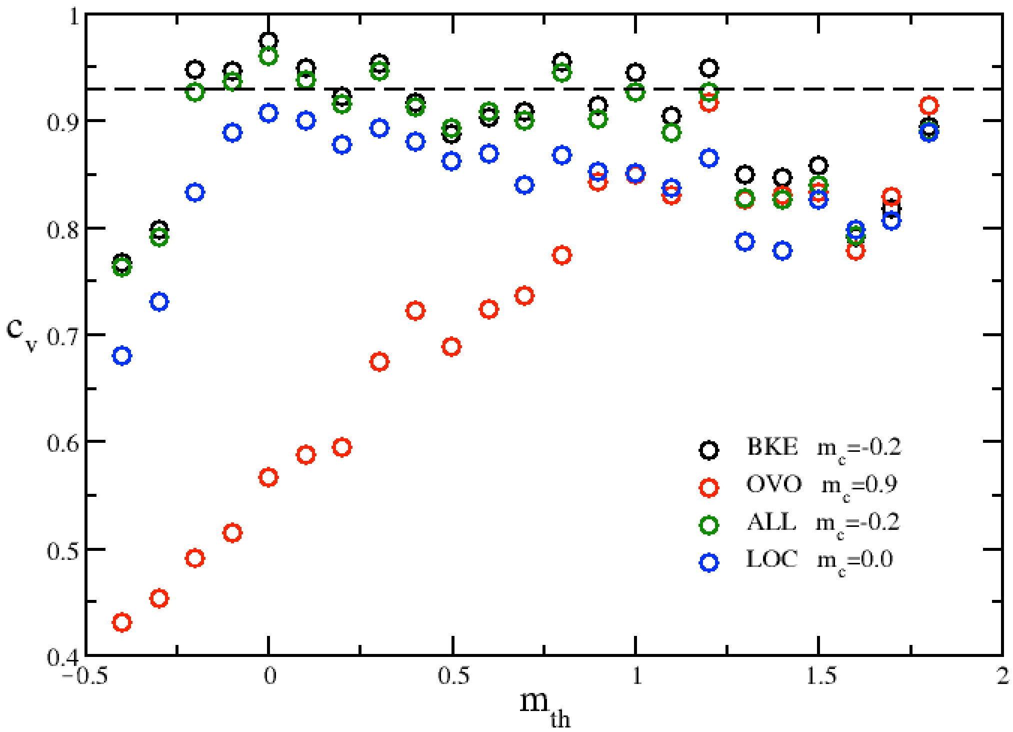

Figure 7. c_V vs. m_{th} for the four catalogues analysed here in the range [−0.5, 1.8].

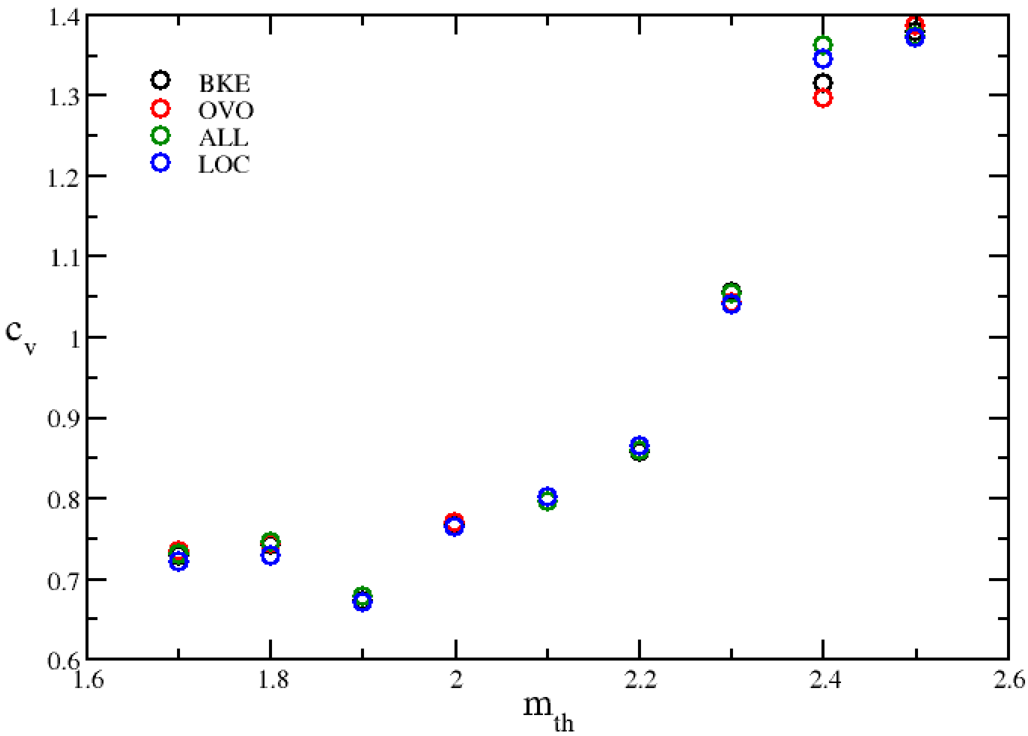

Figure 8. c_V vs. m_{th} for the four catalogues analysed here in the range [1.7, 2.5].

The analysis of c_V, in the two different magnitude intervals confirmed the existence of the two scaling regimes with different *b*-values. This feature appears to be very stable in time. Indeed, the GR distributions for each year (Figure 9) exhibited a double-scaling behaviour (although not very pronounced in some cases), which called for a deeper investigation on the possible causes of the experimental observation.

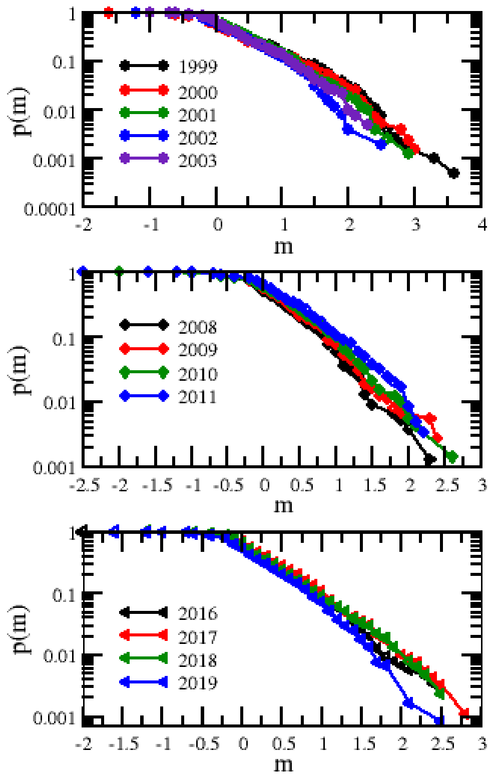

Figure 9. The GR distribution for each year from 1999 to 2023. Here, we limited our analysis to the ALL catalogue because it was the most homogeneous and the longest one among the others.

3.1. The Double Scaling of the *b*-Value: A Physical Effect?

The *b*-value was strongly affected by the properties of the crustal structure; in particular, stress conditions and fluid circulation, which also contributed to determining the patterns of the stress seismic release, in time and space. Thus, in the search for the origin, we first assumed that the observed double scaling in the *b*-value could result from the physical characteristics of the seismogenic volume. Potential sources could be, for instance, a finite size effect or the concurrence of earthquakes occurring in different sectors of the crustal structure, characterized by distinct properties, as also suggested by some authors [81].

As a first possible interpretation of the two scaling regimes characterizing the GR distribution, we checked if this could be attributed to a finite-size effect. Namely, the second (higher *b*) regime could be due to a tapering of the distribution with a faster decay, due to the system reaching its size limit. Following this hypothesis, the seismic energy should follow a Gamma distribution [82,83]. Thus, we transformed the magnitude to the seismic moment (proportional to energy), through the relationship $\log M_0 = 9.8 + 0.8 m_d$ [84]. The existence of two scaling regimes was also confirmed for the M_0 distribution for all of the catalogues (Figure 10), including OVO, revealing that, although hidden by incompleteness problems, the first scaling regime characterized this catalogue too. The existence of two different power law regimes in $p(M_0)$ led us to exclude the finite size effect as a possible explanation for the two scaling regimes in the GR distribution.

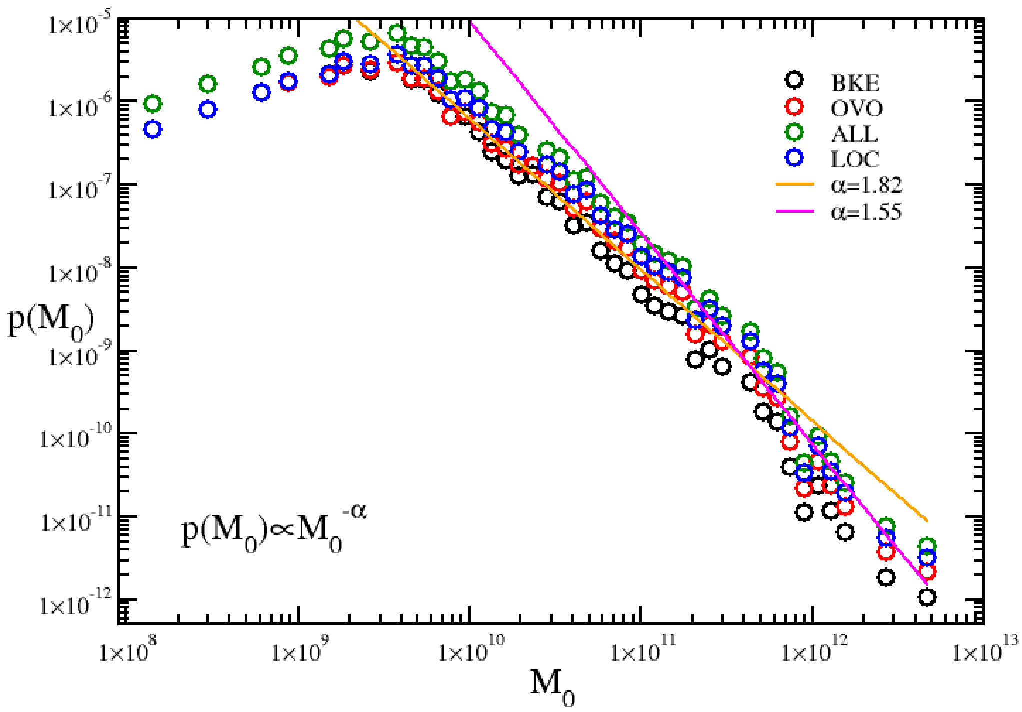

Figure 10. The M_0 distribution. The continuous lines are plotted as a guide for the eyes.

Then, we considered the hypothesis that the two distinct *b*-values could be associated with different earthquake clusters, separated in depth. In fact, two different physical mechanisms were proposed to cause shallow and deep events at Mt. Vesuvius, by indicating the gravitational load within the volcano edifice and a concurrence of regional stress and crustal heterogeneity (in association with the action of hydrothermal fluids) as the main sources of stress for shallow (depth < 1 km) and deep earthquakes [81], respectively.

We verified this possibility by evaluating the GR distribution for subsets of events in the LOC catalogue, either by repeatedly splitting the data according to a depth threshold z_{th}, varying by 0.5 km in a range of 0.5–2.0 km, or by separating the events into 1 km-thick layers. The results indicate that the deeper seismicity assumed smaller *b*-values in all cases (Figure 11), in agreement with previous studies [81] and with the evidence of a larger stress drop for deeper events [84]. The maximum difference in the *b*-value results by splitting the data at the depth threshold of 1 km. In fact, this level marked the separation between two major clusters of earthquakes —with the shallow one corresponding to events occurring inside the volcanic cone—possibly connected with distinct triggering conditions (e.g., [81,84]).

However, we remark that the GR distribution was characterized by double scaling for all of the z_{th} values (Figure 12 and Table 3) and in all the layers (Figure 13), leading us to exclude a depth dependence of *b* as a viable explanation for the observed break in the cumulative earthquake frequency-magnitude distribution.

Table 3. The number of events in the shallower and deeper layers *n*, the *b*-values with their standard deviations for the different z_{th} values.

	Up			Down		
z_{th}	n	b	σ_b	n	b	σ_b
0.5	6086	0.79	9.51×10^{-3}	2711	0.45	5.94×10^{-3}
1.0	6901	0.75	8.45×10^{-3}	1896	0.41	5.91×10^{-3}
1.5	7434	0.71	7.63×10^{-3}	1363	0.40	6.67×10^{-3}
2.0	8038	0.67	6.74×10^{-3}	759	0.41	9.61×10^{-3}

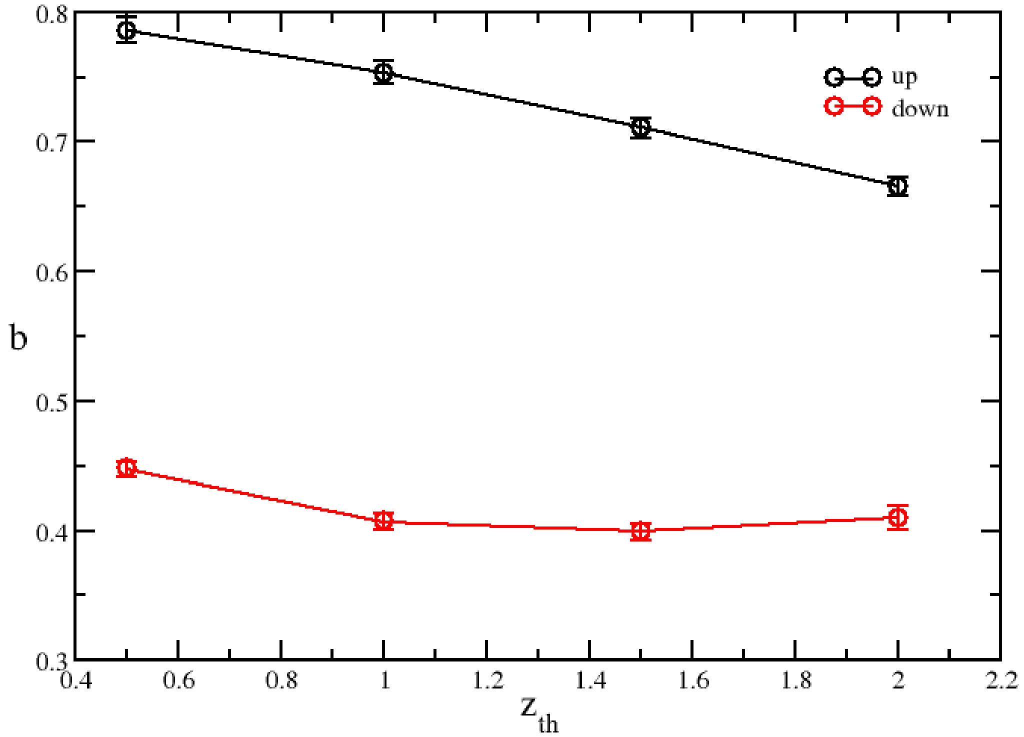

Figure 11. The *b*-values as a function of z_{th}.

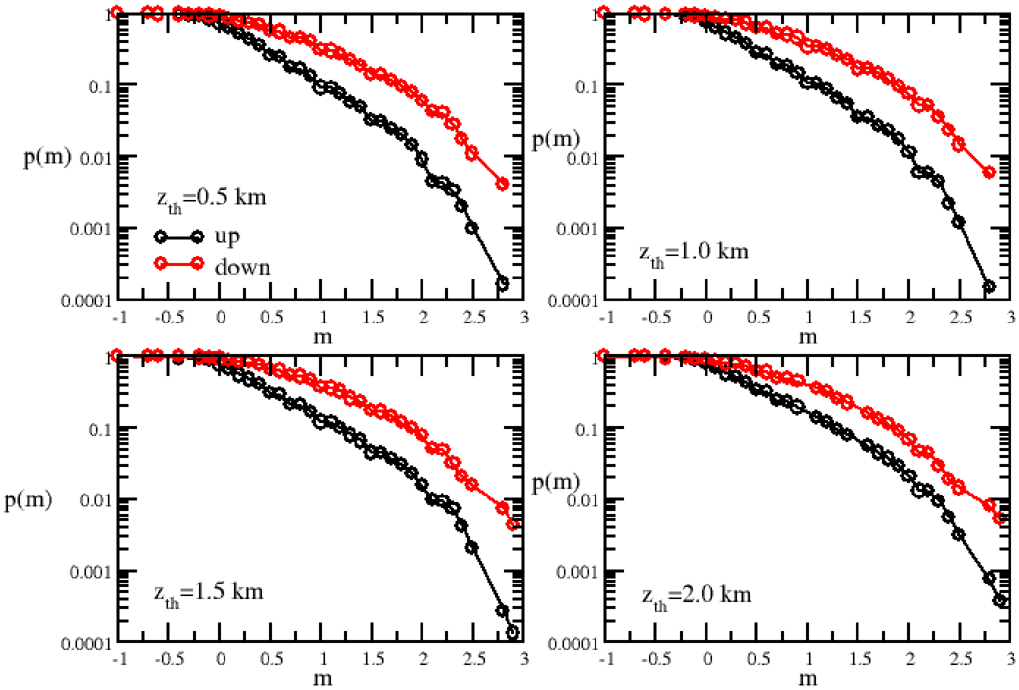

Figure 12. The GR distribution for the LOC catalogue and for the four z_{th} here analyzed.

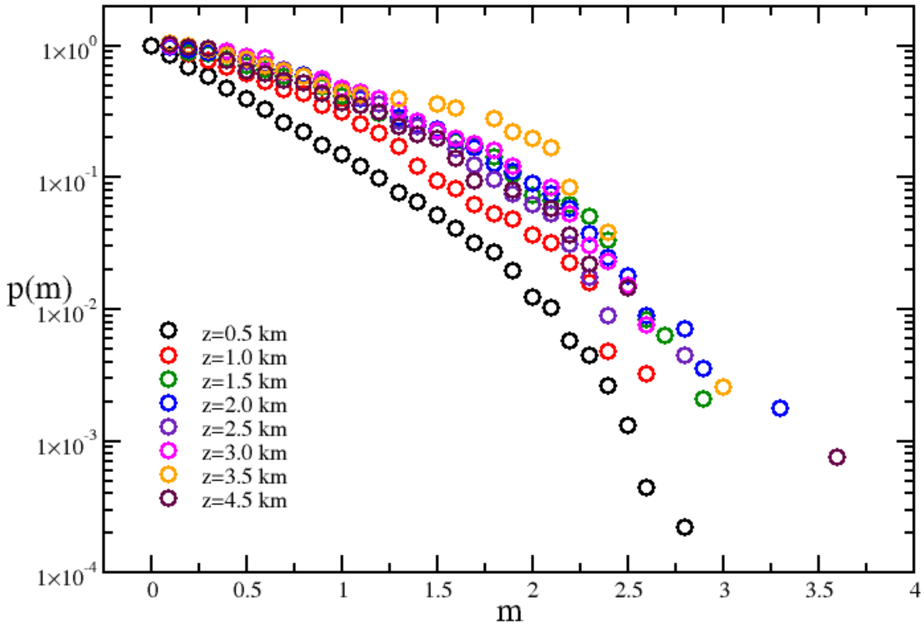

Figure 13. The GR distribution for the LOC catalogue and for the different layers analysed here. The analysis is limited to magnitudes larger than 0.

Then, we investigated the dependence of the magnitude distribution on the distance from the Vesuvius crater (notably, the crater coordinates were extremely close to the average latitude and longitude of the located earthquakes). We separated the entire seismicity into two groups: one including the events inside a circle with a radius of r, centred at the crater, and the other with the remaining ones. As the threshold radius, we tested either the average (d_a) or the median (d_m) of the earthquake distance from the crater. In both cases, the GR law exhibited the same double scaling (Figure 14).

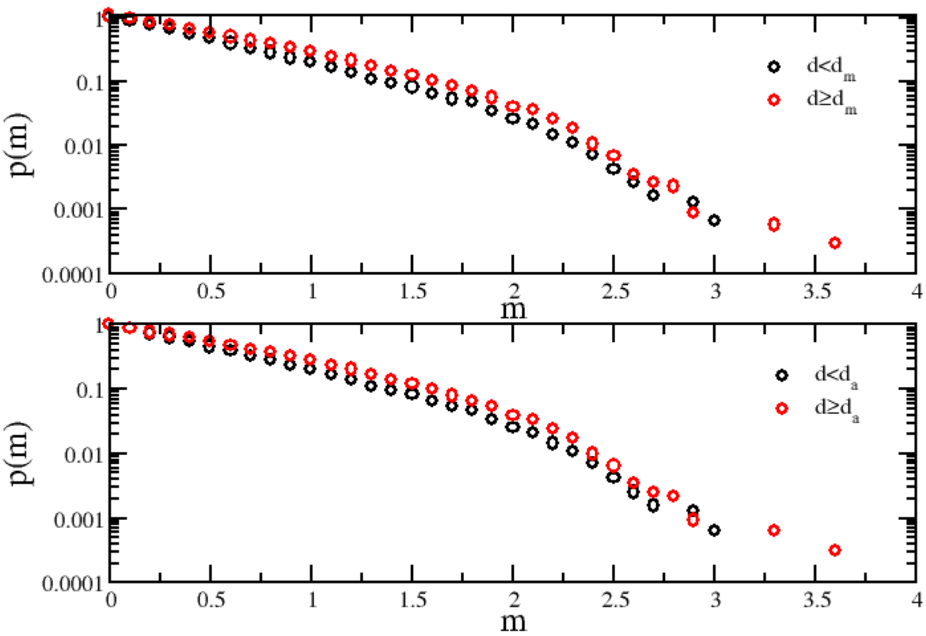

Figure 14. The GR distributions for the two groups of events spatially separated by a circle of radius d_m (**upper panel**) and d_a (**lower panel**).

As a further tentative interpretation, we investigate the possibility that the two-scaling regime could result from the superposition of earthquakes characterized by distinct time clustering. In general, volcano-tectonic earthquakes occur in swarms—i.e., group of small earthquakes concentrated in time and space—or as variable mainshock–aftershocks sequences. Several authors considered that the different characteristics of these two groups might have resulted in distinct *b*-values (e.g., [85]). Therefore, we tested if this was the case for the seismicity of Mt. Vesuvius.

We verified this occurrence by separating the ALL catalogue in events occurring within and outside seismic swarms, respectively. Here, we focused only on the ALL catalogue, which was very similar to BKE, while OVO was almost Poissonian (with only two swarms individuated) and LOC was too scanty for this analysis. The method for individuating the swarms is described in the Appendix A.

The results illustrated in Figure 15 reveal that the GR distribution for both groups of earthquakes was very similar and, again, they were still characterized by the same two-scaling regime.

Apparently, the break of the slope observed in the frequency-magnitude of the Mt. Vesuvius seismicity was persistent with time and could not be explained as the superposition of earthquakes occurring either in distinct volumes or with different time clustering properties. Thus, based on the above analyses, we rejected the possibility that the double scaling in the *b*-value could be a real effect.

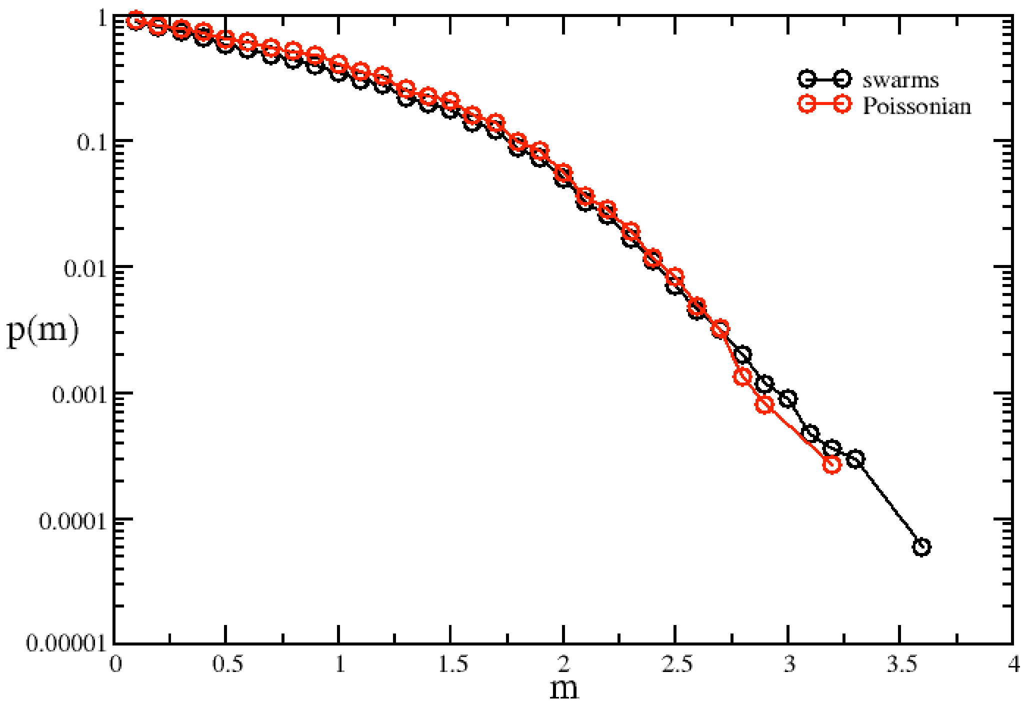

Figure 15. The GR distributions for the clustered and non clustered events for the ALL catalogue.

3.2. The Double Scaling of the b-Value: A Magnitude Uncertainty Effect

The use of the GR distribution for seismic hazard assessment or for deriving indications on the state of stress counted on the reliable determination of the earthquakes' magnitude. For instance, Uchide and Imanishi [86] demonstrated that underestimation of the magnitude for microseismicity influenced earthquake statistics, thus affecting the seismic hazard inferences.

As described above, a duration magnitude m_d for the Mt. Vesuvius seismicity was routinely estimated at the two sites of OVO and BKE, based on a relation derived in early 1980s from earthquakes with $m \geq 3.0$, then extrapolated to lower magnitudes, typical of most earthquakes in this area.

Since then, the local seismic monitoring network run by the Osservatorio Vesuviano, now INGV, has been developed in the number and quality of the instruments for detecting, measuring, and recording the ground motion. Since 1998, Helicorder drums were progressively substituted with video monitors, while the number of station progressively increased since 2004, from 6 to the present 18 (Figure 2). The limited magnitude range for which a reliable duration–magnitude regression could be obtained and the technological changes might have had significant effects on the estimated m_d, possibly mirroring the resulting b-value.

For instance, Iannaccone and co-authors [87] demonstrated that the duration was overestimated by a few seconds, increasing with the waveform duration, when the seismograms were analysed on screen, rather than on drums. Because of the logarithmic dependence on the duration, this was reflected in a larger m_d—the difference exponentially increased with the decreased magnitude—with Δm_d being in excess of 0.1 and 0.2 at m_d = 2.0 and m_d = 1.0, respectively. In principle, being larger for small events, such a difference could determine the presence of a misleading double scaling in the b-value. However, if this was the source, it would require that the duration of a large majority of the events included in the analysed catalogues were estimated on Helicorder drums, whereas the complete transition to video monitor analysis of the seismograms was accomplished by 2000 [88].

Therefore, a different origin needed to be searched. To this aim, we focussed on the analysis of the regressions themselves. As mentioned above, the first duration–magnitude relation for Mt. Vesuvius seismicity was obtained for the OVO station, by comparing the observed duration of the ground motion associated with earthquakes occurring during the 1980–1981 Irpinia seismic sequence—50 to 80 km to E-SE—with the Richter magnitude m_L estimated for the same even from the waveform recorded at a Wood–Anderson seismometer installed about 200 km NE of Vesuvius. The relative location of the sources and the recording sites did not allow for the calibration of earthquakes with a magnitude lower than 3.0; the regression was simply extrapolated to a lower magnitude [74], a procedure that could not ensure the correctness of the estimation at this range. As a matter of fact, Del Pezzo and Petrosino [89] demonstrated that this relation was not appropriate for smaller earthquakes. By using permanent and temporary stations, those authors derived the following relation:

$$m_L = 0.682 + 0.655 \cdot m_d, \tag{3}$$

between the OVO duration magnitude and the BKE local magnitude, for 131 Vesuvius earthquakes, this showed that m_d significantly underestimated m_L at lower magnitudes (Figure 16). According to this relation, the duration magnitude at OVO should be evaluated using [89]:

$$m_d = 1.8 \cdot \log \tau - 0.9. \tag{4}$$

We remark that the results obtained by [89] were well constrained, and were based (i) on the determination of an experimental distance–attenuation curve for Mt. Vesuvius events and (ii) on the simulation of Wood–Anderson seismograms, starting from recordings at a 1 Hz MARK L4-3D installed at BKE. On the other hand, less than 10% of the data analysed by [89] were above $m_d > 2.0$, and it is quite apparent that, beyond this threshold, a simple $m_L = m_d$ regression (i.e., the one obtained by [74]) clearly justified the observations much better than the above relation.

Based on this observation, we split the whole dataset at $m = 2$ and separately fit a linear model to the two groups of data. The regression for $m \geq 2$ resulted very close to $m_L = m_d$, being:

$$m_L = -0.18 + 1.09 \cdot m_d. \tag{5}$$

Conversely, the observation for $m \leq 2$ are described by the following:

$$m_L = 0.74 + 0.57 \cdot m_d, \tag{6}$$

very close to Equation (3), as shown in Figure 16.

The similarity of Equation (1) to Equation (5) implies that the relation derived by [74] for $m_d \geq 3.0$ could be reliably extended down ~ 2.0. At the same time, the difference using Equation (6) evidenced its fallacy for lower magnitudes. Thus, more reliable magnitude estimates for Mt. Vesuvius earthquakes could be obtained by using the relation (1) for $m_d \geq 2.0$ and the regression (6) for a lower magnitude.

On these grounds, we now focussed on the ALL catalogue and modified the magnitude by accounting for the above correction; then, we re-computed the frequency-magnitude distribution.

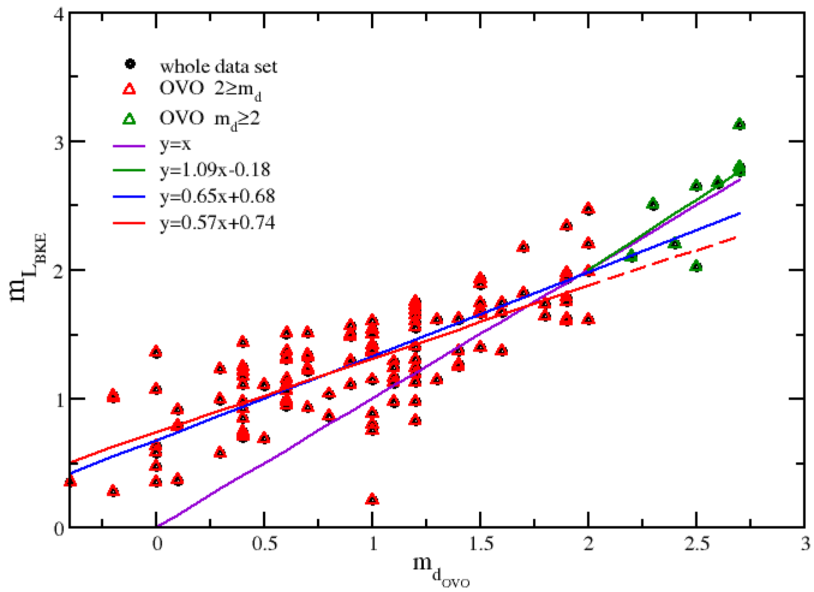

Figure 16. Relation between duration magnitude m_d at OVO and local magnitude m_L at BKE for 131 Vesuvius earthquakes. Data are from [89]. The violet and blue lines correspond to $m_L = m_d$ [74] and $m_L = 0.682 + 0.655 \cdot m_d$ [89], respectively; while the red and green lines represent the linear regression for the points in the corresponding colour.

The corrected catalogue exhibited a more usual GR distribution (Figure 17), with a single, well defined, m_c and a higher b-value, as generally observed in volcanic areas [90–92]. All of the above evidence strongly suggest that the break in magnitude scaling was not a real effect, rather it resulted from an arbitrary, inappropriate, extension of the regressions (1) and (2) to lower magnitudes. In order to retain the homogeneity of the catalogue, a change in the relation routinely used for the magnitude estimation is not recommended; however, we emphasize that caution should be provided when the seismic catalogues available for Mt. Vesuvius are used for investigating the time and space variations in the b-value. The relatively scarce level of the local seismicity would force the use of lower magnitude events in this kind of analysis, but their use appeared to not be appropriate below $m \sim 2.0$, if the magnitude was assumed as it was in the catalogues.

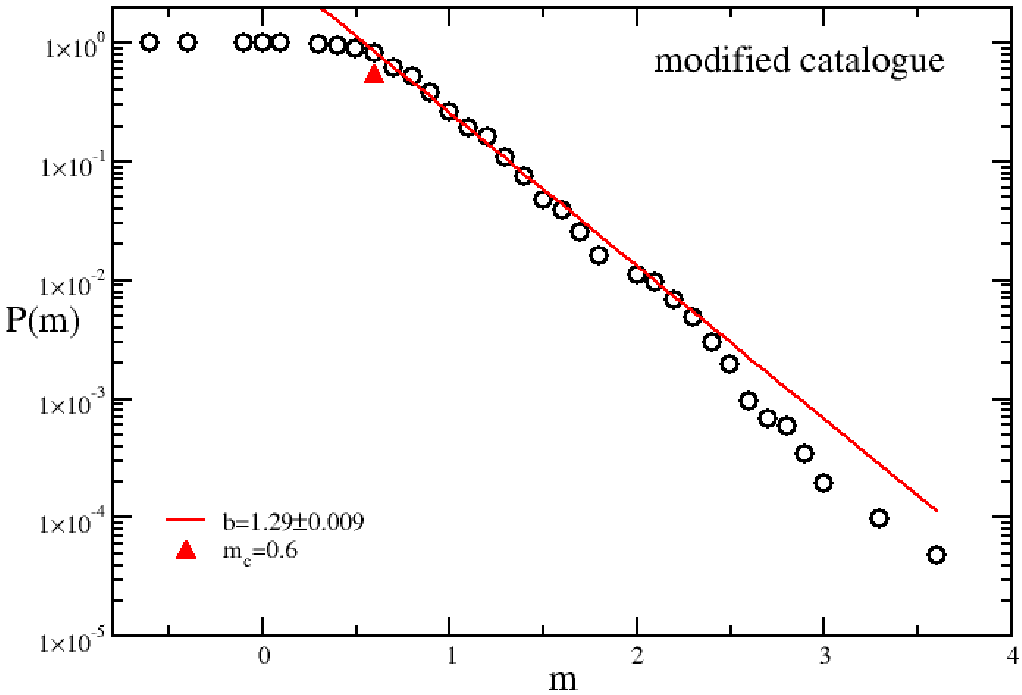

Figure 17. The GR distributions for of the ALL catalogue modified accordingly to relationship (6). The m_c value has been estimated using the c_V method.

4. Time Variation of the *b*-Value and Temporal Clustering Properties

Once we correct for the bias in the magnitude estimation of the low energy events, we reevaluated the GR distribution throughout the considered time period and determined the time variations in the b value: an important tool for investigating the stress state changes with time. In addition, we also analysed the time variations of m_c, the average time interval between two successive events $\langle \Delta t \rangle$, and the Δt variability coefficient $c_V^{(\Delta t)}$, defined as

$$c_V^{(\Delta t)} = \frac{\sigma_{\Delta t}}{\langle \Delta t \rangle}, \tag{7}$$

where $\sigma_{\Delta t}$ is the Δt standard deviation. This $c_V^{(\Delta t)}$ should not be confused with the c_V previously used in estimating m_c. Indeed, that is the magnitude variability coefficient, while here the $c_V^{(\Delta t)}$ of Δt describes the time clustering properties of the seismicity; it assumes a value of 1 when the earthquake occurrence is Poissonian and larger values when events cluster in time. It is worth recalling that the $c_V^{(\Delta t)}$ depends on the time of occurrence of earthquakes; thus, in principle, its analysis might be influenced by the assumed magnitude definition, affecting the m_c value.

Figure 18 shows the four parameters as a function of time. m_c was almost fixed at the two values of 0.6 and 0.7, in very good agreement with what was found for the whole catalogue. The b value exhibited a slight increase with time, indicating a possible decrease in stress on the volcano edifice. After removing the trend, b fluctuated around 1.4, confirming the results obtained for the whole catalogue. The b distribution was very close to a Gaussian one (Figure 19), whose standard deviation (0.13) was close to the average estimation error of b (0.08). This ensured that these fluctuations were purely random and not linked to the volcano dynamics. Also, $\langle \Delta t \rangle$ exhibited few significant variations in fluctuation, within the standard deviation, around $\simeq$18 h. On the other hand, $c_V^{(\Delta t)}$ varied between 0.9 and 1.9; however, a great part of the $c_V^{(\Delta t)}$ values fluctuated in the range of [1.1, 1.4], indicating a weak clustering degree (see the average rate of occurrence in the Appendix A). $c_V^{(\Delta t)}$ assumed larger values corresponding with larger swarms.

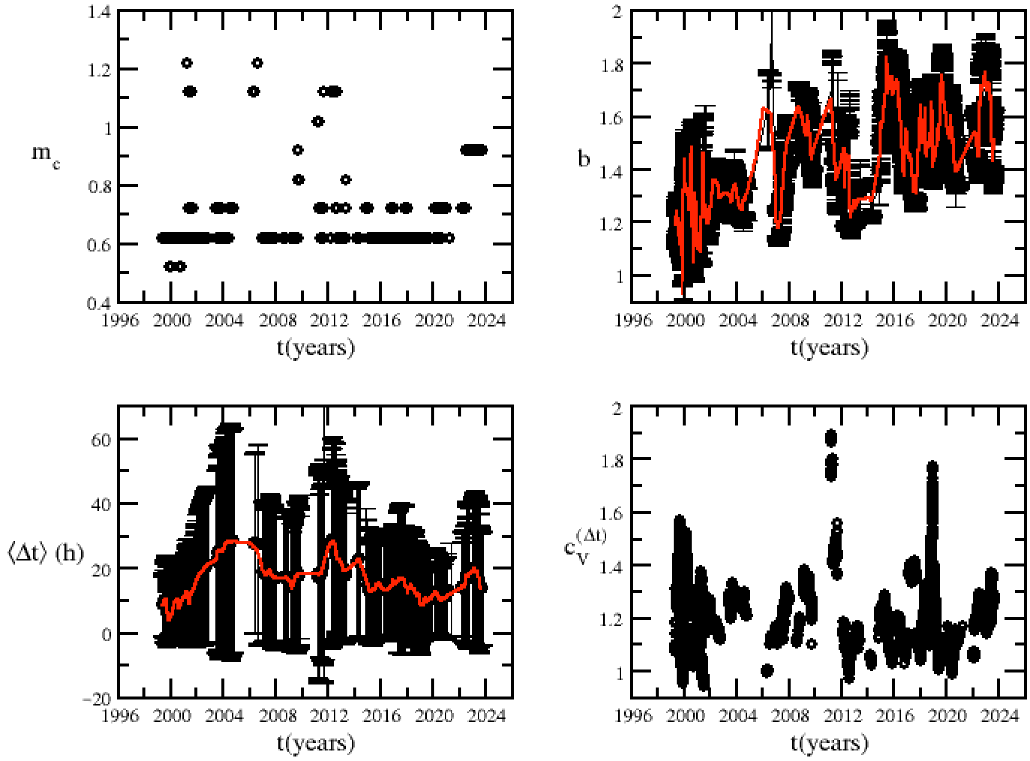

Figure 18. m_c , b-value, $\langle \Delta \text{ t} \rangle$ and $c_V^{(\Delta t)}$ as a function of time, for the modified magnitude catalogue.

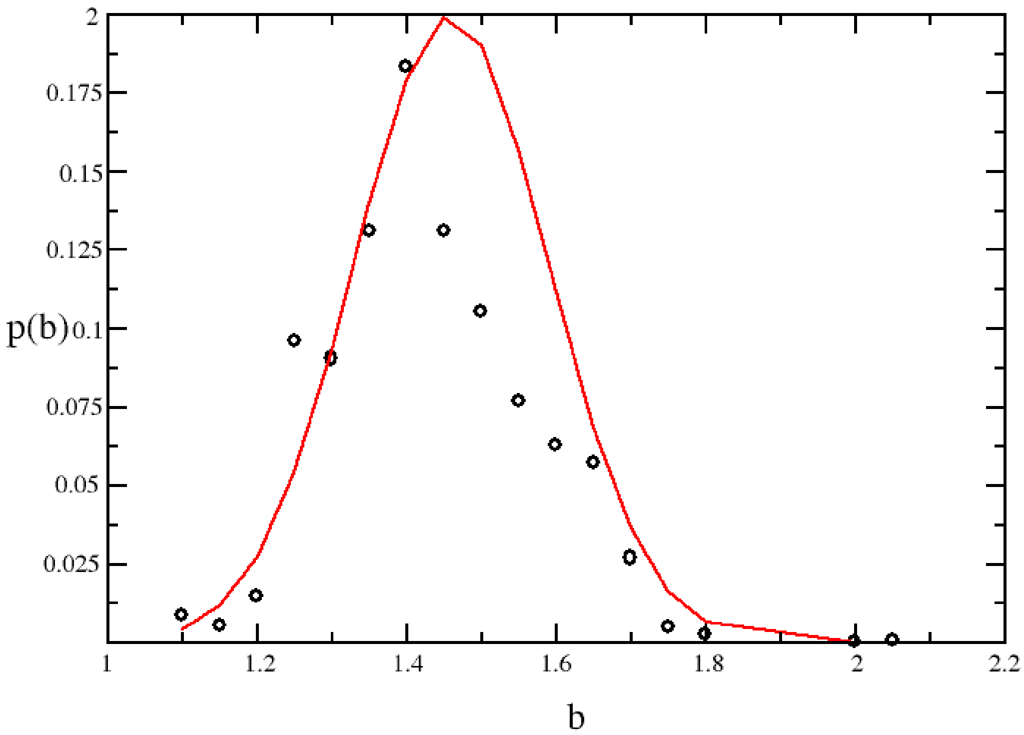

Figure 19. The b-value distribution.

The stationary behaviour of the analysed statistical parameters is a clear indication that the volcano state had not changed during the last 40 years. The only exception was represented by the occurrence of small swarms rapidly expiring (see Appendix A).

5. Conclusions

We analysed the seismicity of the Vesuvius volcano investigating the statistical characteristics of three different catalogues. The GR distribution appeared to be characterized by the presence of two scaling regimes unusual for the standard GR distribution. Here, we tested four different possible origins for this effect: (i) a finite size effect, (ii) depth variations of the b-value, (iii) a b-value depending on the distance from the crater area, and (iv) different b-value for time clustered and non-clustered events. None of these hypotheses are able to account for the double scaling regime of the GR distribution. As a consequence, we maintained that there was a bias in the magnitude. In particular, we suggest that the adopted duration–magnitude linear regression at the base of the catalogue, and originally determined for $m \geq 3.0$, cannot be extrapolated to smaller magnitudes. Thus, we derived a different relation between m_L and m_d, for earthquakes with $m \leq 2.0$, by using the data estimates by [89], and we corrected the catalogue magnitudes accordingly. When the correction was applied, the GR distribution assumed the usual shape and the resulting b was similar to the values usually observed in volcanic areas [90–92].

We also investigated the time variation of four statistical parameters: b-value, m_c, $\langle \Delta t \rangle$, and $c_V^{(\Delta t)}$. Our analysis indicates that the magnitude of completeness m_c was not strongly affected by the evolution of the seismic network. This result was associated with the very localized nature of the seismicity around the crater axis, allowing for a good level of detection, even with the first, sparse network configurations. Similarly, the average time interval between successive earthquakes $\langle \Delta t \rangle$ exhibited an approximately stationary behaviour, revealing that the time occurrence of seismicity at Mt. Vesuvius had not changed significantly in the last decades. The small changes of $c_V^{(\Delta t)}$, excluding the abrupt increase in the correspondence of the three largest swarms, confirmed this result.

The analysis of the occurrence rate of the events within the swarms evidenced a sharp decrease with time (Figure A2), indicating the overall short duration for most of the almost 400 swarms, generally characterized by 10–20 earthquakes, with only 21 having more than 50 events.

Finally, the average Gutenberg–Richter b-values slightly increased during the entire analysed period, suggesting a slow, but continuous reduction in differential stress within the volcano edifice, possibly following the 1999 swarm, associated with the strongest earthquake (9 October 1999; m_d = 3.6) since the last eruption in 1944–1945 .

Author Contributions: All of the authors provided the same contribution to all parts of the manuscript. All authors have read and agreed to the published version of the manuscript.

Funding: This research received no external funding.

Data Availability Statement: The earthquake catalogues used in the present study are available from INGV-Osservatorio Vesuviano, at https://www.ov.ingv.it, accessed on 28 November 2023.

Acknowledgments: We are grateful to Simona Petrosino for providing the estimates of the magnitude m_d at OVO and of the local magnitude m_L at BKE for 131 Vesuvius earthquakes.

Conflicts of Interest: The authors declare that they have no conflicts of interest. This research would be used only for scientific research and would not be passed on to third parties.

Appendix A. The Inter-Event Time Distribution and the Identification of the Swarms

As mentioned in the introduction, the distribution of the inter-event time Δt between two successive earthquakes represents a powerful tool to investigate the clustering properties of seismic catalogues. Generally, Δt follows the Gamma distribution [50–54]:

$$p(\Delta t) = \frac{1}{\theta^k \Gamma(k)} \Delta t^{k-1} e^{-\frac{\Delta t}{\theta}} \tag{A1}$$

where k controls the Δt decay at small Δt and is linked to the decay of the events rate in the earthquake sequences, θ is the Δt value beyond which the exponential decay becomes dominant. It can be considered as the Δt value separating clustered events from the Poissonian ones. Figure A1 shows the $p(\Delta t)$ for the ALL catalogue. Here, we focus only on that catalogue because BKE is practically the same, OVO is almost Poissonian (only two swarms are individuated), and LOC is too short.

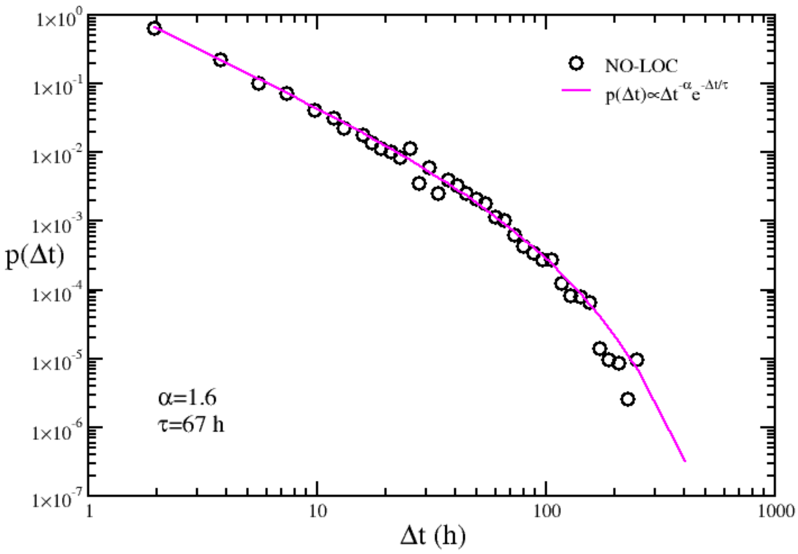

Figure A1. The Δt distribution for ALL catalogue.

The distribution reveals that for $\Delta t < 67$ h, the events should be considered as occurring in clusters (swarms), whereas for $\Delta t > 67$ h, the events are Poissonian.

In order to separate the clustered from Poissonian events, we firstly removed all the events with $m < m_c = -0.2$ from the ALL catalogue, then we defined a swarm when Δt < 67 h and it remained active until Δt was again larger than 67 h. As a further condition, we considered only considered swarms including at least 10 earthquakes as "true". These criteria individuate 368 swarms and 1462 Poissonian events. Therefore, for each swarm i, we evaluate the rate of occurrence R_i defined as the number of earthquakes per 10 h and stack all the rates in a sort of average swarm occurrence rate $\nu(\tau)$, obtaining an exponential decay with time (Figure A2).

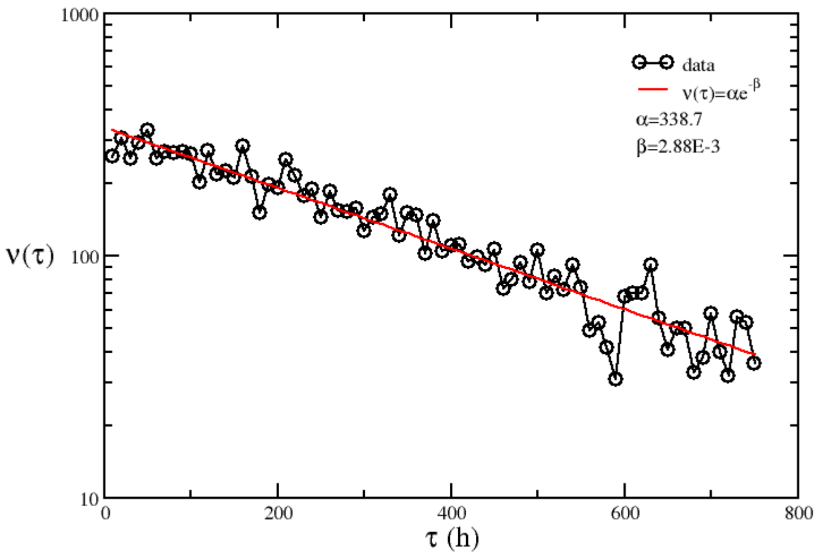

Figure A2. The swarm occurrence rate as a function of time elapsed from the beginning of the swarm τ. The red line is the exponential fit.

References

1. Cusano, P.; Ricco, C.; Aquino, I.; Petrosino, S. A First Step towards the Definition of a Link between Ground Tilt and Earthquakes at Mt. Vesuvius (Italy). *Appl. Sci.* **2022**, *12*, 12261. [CrossRef]
2. Zollo, A.; Gasparini, P.; Virieux, J.; Le Meur, H.; De Natale, G.; Biella, G.; Boschi, E.; Capuano, P.; De Franco, R.; Dell'Aversana, P.; et al. Seismic evidence for a low-velocity zone in the upper crust beneath Mount Vesuvius. *Science* **1996**, *274*, 592–594. [CrossRef]
3. Auger, E.; Gasparini, P.; Virieux, J.; Zollo, A. Seismic evidence of an extended magmatic sill under Mt. Vesuvius. *Science* **2001**, *294*, 1510–1512. [CrossRef] [PubMed]
4. Chiodini, G.; Marini, L.; Russo, M. Geochemical evidence for the existence of high-temperature hydrothermal brines at Vesuvio volcano, Italy. *Geochim. Cosmochim. Acta* **2001**, *65*, 2129–2147. [CrossRef]
5. Del Pezzo, E.; Chiodini, G.; Caliro, S.; Bianco, F.; Avino, R. New insights into Mt. Vesuvius hydrothermal system and its dynamic based on a critical review of seismic tomography and geochemical features. *Ann. Geophys.* **2013**, S0444. [CrossRef]
6. Del Pezzo, E.; Bianco, F.; Saccorotti, G. Duration Magnitude Uncertainty due to Seismic Noise: Inferences on the Temporal Pattern of G-R b-value at Mt. Vesuvius, Italy. *Bull. Seismol. Soc. Am.* **2003**, *93*, 1847–1853. [CrossRef]
7. D'Auria, L.; Massa, B.; Matteo, A.D. The stress field beneath a quiescent stratovolcano: The case of Mount Vesuvius. *J. Geophys. Res. Solid Earth* **2014**, *119*, 1181–1199. [CrossRef]
8. Gutenberg, B.; Richter, C. Frequency of earthquakes in California. *Bull. Seismol. Soc. Am.* **1944**, *34*, 185–188. [CrossRef]
9. Scholz, C. The frequency-magnitude relation of microfracturing in rock and its relation to earthquakes. *Bull. seism. Soc. Am.* **1968**, *58*, 399–415. [CrossRef]
10. Wyss, M. Towards a Physical Understanding of the Earthquake Frequency Distribution. *Geophys. J. R. Astron. Soc.* **1973**, *31*, 341–359. [CrossRef]
11. Amitrano, D. Brittle-ductile transition and associated seismicity: Experimental and numerical studies and relationship with the b value. *J. Geophys. Res. Solid Earth* **2003**, *108*, 2044. [CrossRef]
12. Gulia, L.; Wiemer, S. The influence of tectonic regimes on the earthquake size distribution: A case study for Italy. *Geophys. Res. Lett.* **2010**, *37*, L10305. [CrossRef]
13. Schorlemmer, D.; Wiemer, S.; Wyss, M. Variations in earthquake-size distribution across different stress regimes. *Nature* **2005**, *437*. [CrossRef] [PubMed]
14. Wiemer, S.; Wyss, M. Mapping the frequency-magnitude distribution in asperities:An improved technique to calculate recurrence times? *J. Geophys. Res.* **1997**, *102*, 15115–15128. [CrossRef]
15. Wiemer, S.; Wyss, M. Mapping spatial variability of the frequency-magnitude distribution of earthquakes. *Adv. Geophys.* **2002**, *45*, 259–302.
16. Westerhaus, M.; Wyss, M.; Yilmaz, R.; Zschau, J. Correlating variations of b values and crustal deformations during the 1990s may have pinpointed the rupture initiation of the Mw = 7.4 Izmit earthquake of 1999 August 17. *Geophys. J. Int.* **2002**, *148*, 139–152. [CrossRef]
17. Pino, N.A.; Convertito, V.; Godano, C.; Piromallo, C. Subduction age and stress state control on seismicity in the NW Pacific subducting plate. *Sci. Rep.* **2022**, *12*, 12440. [CrossRef]
18. Tormann, T.; Wiemer, S.; Mignan, A. Systematic survey of high-resolution b value imaging along Californian faults: Inference on asperities. *J. Geophys. Res. Solid Earth* **2014**, *119*, 2029–2054. [CrossRef]
19. Cochran, E.S.; Page, M.T.; van der Elst, N.J.; Ross, Z.E.; Trugman, D.T. Fault Roughness at Seismogenic Depths and Links to Earthquake Behavior. *Seism. Rec.* **2023**, *3*, 37–47. [CrossRef]
20. Collettini, C.; Barchi, M.R.; De Paola, N.; Trippetta, F.; Tinti, E. Rock and fault rheology explain differences between on fault and distributed seismicity. *Nat. Commun.* **2022**, *13*, 5627. [CrossRef]
21. Wiemer, S.; McNutt, S.R. Variations in the frequency-magnitude distribution with depth in two volcanic areas: Mount St. Helens, Washington, and Mt. Spurr, Alaska. *Geophys. Res. Lett.* **1997**, *24*, 189–192. [CrossRef]
22. Wiemer, S.; McNutt, S.R.; Wyss, M. Temporal and three-dimensional spatial analyses of the frequency–magnitude distribution near Long Valley Caldera, California. *Geophys. J. Int.* **1998**, *134*, 409–421. [CrossRef]
23. Murru, M.; Console, R.; Falcone, G.; Montuori, C.; Sgroi, T. Spatial mapping of the b value at Mount Etna, Italy, using earthquake data recorded from 1999 to 2005. *J. Geophys. Res. Solid Earth* **2007**, *112*, B12303. [CrossRef]
24. Suyehiro, S.; Sekiya, H. Foreshocks and earthquake prediction. *Tectonophysics* **1972**, *14*, 219–225. [CrossRef]
25. Papazachos, B.C. The time distribution of reservoir-associated foreshocks and its importance to the prediction of the principal shock. *Bull. Seismol. Soc. Am.* **1973**, *63*, 1973–1978. [CrossRef]
26. Papazachos, B. Foreshocks and earthquake prediction. *Tectonophysics* **1975**, *28*, 213–226. [CrossRef]
27. Ogata, Y.; Utsu, T.; Katsura, K. Statistical discrimination of foreshocks from other earthquake clusters. *Geophys. J. Int.* **1996**, *127*, 17–30. [CrossRef]
28. Papadopoulos, G.; Minadakis, G.; Orfanogiannaki, K. Short-Term Foreshocks and Earthquake Prediction. In *Pre-Earthquake Processes*; American Geophysical Union: Washington, DC, USA, 2018; Chapter 8, pp. 125–147. [CrossRef]
29. Enescu, B.; Ghita, C.; Moldovan, I.-A.; Radulian, M. Revisiting Vrancea (Romania) Intermediate-Depth Seismicity: Some Statistical Characteristics and Seismic Quiescence Testing. *Geosciences* **2023**, *13*, 219. [CrossRef]
30. Gulia, L.; Wiemer, S. Real-time discrimination of earthquake foreshocks and aftershocks. *Nature* **2019**, *574*, 193–199. [CrossRef]

31. Gulia, L.; Rinaldi, A.P.; Tormann, T.; Vannucci, G.; Enescu, B.; Wiemer, S. The Effect of a Mainshock on the Size Distribution of the Aftershocks. *Geophys. Res. Lett.* **2018**, *45*, 13277–13287. [CrossRef]
32. Hainzl, S.; Fischer, T.; Dahm, T. Seismicity-based estimation of the driving fluid pressure in the case of swarm activity in Western Bohemia. *Geophys. J. Int.* **2012**, *191*, 271–281. [CrossRef]
33. White, R.; McCausland, W. Volcano-Tectonic Earthquakes: A new tool for estimating intrusive volumes and forecasting eruptions. *J. Volcanol. Geotherm. Res.* **2015**, *309*, 139–155. [CrossRef]
34. Hainzl, S.; Fischer, T. Indications for a successively triggered rupture growth underlying the 2000 earthquake swarm in Vogtland/NW Bohemia. *J. Geophys. Res. Solid Earth* **2002**, *107*, ESE 5–1–ESE 5–9. [CrossRef]
35. Tramelli, A.; Godano, C.; Ricciolino, P.; Giudicepietro, F.; Caliro, S.; Orazi, M.; De Martino, P.; Chiodini, G. Statistics of seismicity to investigate the Campi Flegrei caldera unrest. *Sci. Rep.* **2021**, *11*, 7211. [CrossRef] [PubMed]
36. Mogi, K. Some Discusions on Aftershocks, Foreshocks and Earthquake Swarms: The Fracture of a Semi-Infinite Body Caused by Inner Stress Origin and Its Relation to the Earthquake Phenomena (3rd Paper). *Bull. Earthq. Res. Inst.* **1963**, *41*, 615–658.
37. Miller, S.A.; Collettini, C.; Chiaraluce, L.; Cocco, M.; Barchi, M.; Kaus, B.J.P. Aftershocks driven by a high-pressure CO2 source at depth. *Nature* **2004**, *427*, 724–727. [CrossRef] [PubMed]
38. Chouet, B.A. Long-period volcano seismicity: Its source and use in eruption forecasting. *Nature* **1996**, *380*, 309–316. [CrossRef]
39. Toda, S.; Stein, R.; Sagiya, T. Evidence from the AD 2000 Izu islands earthquake swarm that stressing rate governs seismicity. *Nature* **2002**, *419*, 58–61. [CrossRef]
40. Hainzl, S. Self-organization of earthquake swarms. *J. Geodyn.* **2003**, *35*, 157–172. [CrossRef]
41. Glazner, A.F.; McNutt, S.R. Relationship Between Dike Injection and b-Value for Volcanic Earthquake Swarms. *J. Geophys. Res. Solid Earth* **2021**, *126*, e2020JB021631. [CrossRef]
42. Ogata, Y. Statistical Models for Earthquake Occurrences and Residual Analysis for Point Processes. *Res. Memo. Tech. Rep. Inst. Stat. Math. Tokyo* **1985**, *288*, 9–27. [CrossRef]
43. Ogata, Y. Space-time point-process models for earthquake occurrences. *Ann. Inst. Stat. Math.* **1998**, *50*, 379–402. [CrossRef]
44. Marsan, D.; Prono, E.; Helmstetter, A. Monitoring aseismic forcing in fault zones using earthquake time series. *Bull. Seismol. Soc. Am.* **2013**, *103*, 169–179. [CrossRef]
45. Reverso, T.; Marsan, D.; Helmstetter, A. Detection and characterization of transient forcing episodes affecting earthquake activity in the Aleutian Arc system. *Earth Planet. Sci. Lett.* **2015**, *412*, 25–34. [CrossRef]
46. Kattamanchi, S.; Tiwari, T.R.K.; Ramesh, D.S. Non-stationary ETAS to model earthquake occurrences affected by episodic aseismic transients. *Earth Planets Space* **2017**, *69*, 157. [CrossRef]
47. Lombardi, A.M.; Marzocchi, W.; Selva, J. Exploring the evolution of a volcanic seismic swarm: The case of the 2000 Izu Islands swarm. *Geophys. Res. Lett.* **2006**, *33*. [CrossRef]
48. Omori, F. On the after-shocks of earthquakes. *J. Coll. Sci. Imp. Univ. Tokyo* **1894**, *7*, 111–200.
49. Godano, C.; Tramelli, A.; Mora, M.; Taylor, W.; Petrillo, G. An Analytic Expression for the Volcanic Seismic Swarms Occurrence Rate. A Case Study of Some Volcanoes in the World. *Earth Space Sci.* **2023**, *10*, e2022EA002534. [CrossRef]
50. de Arcangelis, L.; Godano, C.; Grasso, J.R.; Lippiello, E. Statistical physics approach to earthquake occurrence and forecasting. *Phys. Rep.* **2016**, *628*, 1–91. [CrossRef]
51. Corral, A. Local distributions and rate fluctuations in a unified scaling law for earthquakes. *Phys. Rev. E* **2003**, *68*, 035102. [CrossRef]
52. Corral, A. Long-Term Clustering, Scaling, and Universality in the Temporal Occurrence of Earthquakes. *Phys. Rev. Lett.* **2004**, *92*, 108501. [CrossRef] [PubMed]
53. Corral, A. Dependence of earthquake recurrence times and independence of magnitudes on seismicity history. *Tectonophysics* **2006**, *424*, 177–193. [CrossRef]
54. Enescu, B.; Struzik, Z.; and Kiyono, K. On the recurrence time of earthquakes: Insight from Vrancea (Romania) intermediate-depth events. *Geophys. J. Int.* **2008**, *172*, 395–404. [CrossRef]
55. Corral, A. Statistical tests for scaling in the inter-event times of earthquakes in California. *Int. J. Mod. Phys. B* **2009**, *23*, 5570–5582. [CrossRef]
56. Shcherbakov, R.; Yakovlev, G.; Turcotte, D.L.; Rundle, J.B. Model for the Distribution of Aftershock Interoccurrence Times. *Phys. Rev. Lett.* **2005**, *95*, 218501. [CrossRef] [PubMed]
57. Bottiglieri, M.; Lippiello, E.; Godano, C.; De Arcangelis, L. Comparison of branching models for seismicity and likelihood maximization through simulated annealing. *J. Geophys. Res. Space Phys.* **2011**, *116*, B02303. [CrossRef]
58. Lindman, M.; Jonsdottir, K.; Roberts, R.; Lund, B.; Bödvarsson, R. Earthquakes Descaled: On Waiting Time Distributions and Scaling Laws. *Phys. Rev. Lett.* **2005**, *94*, 108501. [CrossRef]
59. Molchan, G. Interevent Time Distribution in Seismicity: A Theoretical Approach. *Pure Appl. Geophys.* **2005**, *162*, 1135–1150. [CrossRef]
60. Hainzl, S.; Scherbaum, F.; Beauval, C. Estimating Background Activity Based on Interevent-Time Distribution. *Bull. Seismol. Soc. Am.* **2006**, *96*, 313–320. [CrossRef]
61. Saichev, A.; Sornette, D. "Universal" Distribution of Interearthquake Times Explained. *Phys. Rev. Lett.* **2006**, *97*, 078501. [CrossRef]
62. Saichev, A.; Sornette, D. Theory of earthquake recurrence times. *J. Geophys. Res. Solid Earth* **2007**, *112*, B04313. [CrossRef]

63. Sornette, D.; Utkin, S.; Saichev, A. Solution of the nonlinear theory and tests of earthquake recurrence times. *Phys. Rev. E* **2008**, *77*, 066109. [CrossRef] [PubMed]
64. Touati, S.; Naylor, M.; Main, I.G. Origin and Nonuniversality of the Earthquake Interevent Time Distribution. *Phys. Rev. Lett.* **2009**, *102*, 168501. [CrossRef]
65. Bottiglieri, M.; de Arcangelis, L.; Godano, C.; Lippiello, E. Multiple-Time Scaling and Universal Behavior of the Earthquake Interevent Time Distribution. *Phys. Rev. Lett.* **2010**, *104*, 158501. [CrossRef]
66. Godano, C. A new expression for the earthquake interevent time distribution. *Geophys. J. Int.* **2015**, *202*, 219–223. [CrossRef]
67. Bottiglieri, M.; De Martino, S.; Falanga, M.; Godano, C.; Palo, M. Statistics of inter-time of Strombolian explosion-quakes. *EPL (Europhys. Lett.)* **2005**, *72*, 493. [CrossRef]
68. Palmieri, L. Catalogo delle scosse di terremoto segnate dal sismografo elettro-magnetico all'Osservatorio Vesuviano durante i mesi di Dicembre 1861, e Gennaio 1862, in occasione dell'eruzione del Vesuvio cominciata il dì 8 Dicembre, col riscontro di alcune osservazioni meteorologiche contemporanee. *Cron. Del Vesuvio Ann. Del R Oss. Meteorol. Vesuv. Anno* **1862**, *2*, 1–20.
69. Casertano, L. I sismi vesuviani (9 Aprile 1944–31 Dicembre 1956). *Ann. Oss. Vesuviano Ser.* **1956**, *2*, 190–204.
70. Casertano, L. Su analisi di registrazioni di sismi vesuviani. *Ann. Oss. Vesuviano Ser.* **1956**, *2*, 180–189.
71. Casertano, L. I sismi vesuviani dal 1° Gennaio 1957 al 31 Dicembre 1964. In *Atti del XVI Convegno Annuale*; Consiglio Nazionale delle Ricerche: Roma, Italy, 1968; pp. 289–300.
72. Lo Bascio, D.; Ricciolino, P. Cataloghi Sismici dei Vulcani Campani. Stazione BKE Vesuvio dal 1999 al 2021. Available online: https://www.ov.ingv.it/index.php/monitoraggio-sismico-e-vulcanico-2/banche-dati?id=217 (accessed on 28 November 2023).
73. Ricciolino, P.; Lo Bascio, D. Cataloghi Sismici dei Vulcani Campani. Stazione OVO Vesuvio dal 1972 al 2021. Available online: https://www.ov.ingv.it/index.php/monitoraggio-sismico-e-vulcanico-2/banche-dati?id=217 (accessed on 28 November 2023).
74. Scarpa, R. Il terremoto campano-lucano del 23.11.1980: Elaborazione dei dati sismometrici. *Rend. Soc. Geol. It.* **1981**, *4*, 427–450.
75. Wiemer, S.; Wyss, M. Minimum Magnitude of Completeness in Earthquake Catalogs: Examples from Alaska, the Western United States, and Japan. *Bull. Seismol. Soc. Am.* **2000**, *90*, 859–869. [CrossRef]
76. Cao, A.; Gao, S.S. Temporal variation of seismic b-values beneath northeastern Japan island arc *Geophys. Res. Lett.* **2002**, *29*, 48-1–48-3. [CrossRef]
77. Ogata, Y.; Katsura, K. Analysis of temporal and spatial heterogeneity of magnitude frequency distribution inferred from earthquake catalogues. *Geophys. J. Int.* **1993**, *113*, 727–738.
78. Godano, C. A new method for the estimation of the completeness magnitude. *Phys. Earth Planet. Inter.* **2017**, *263*, 7–11. [CrossRef]
79. Godano, C.; Petrillo, G. Estimating the completeness magnitude mc and the b-values in a snap. *Earth Space Sci.* **1993**, *10*, e2022EA002540. [CrossRef]
80. Godano, C.; Petrillo, G.; Lippiello, E. Evaluating the incompleteness magnitude using an unbiased estimate of the *b* value. *Geophys. J. Int.* **2024**, *236*, 994–1001. [CrossRef]
81. D'Auria, L.; Esposito, A.M.; Lo Bascio, D.; Ricciolino, P.; Giudicepietro, F.; Martini, M.; Caputo, T.; De Cesare, W.; Orazi, M.; Peluso, R.; et al. The recent seismicity of Mt. Vesuvius: Inference on seismogenic processes. *Ann. Geophys.* **2013**, *56*, S0442.
82. Serafino, M.; Cimini, G.; Maritan, A.; Rinaldo, A.; Suweis, S.; Banavar, J.R.; Caldarelli, G. True scale-free networks hidden by finite size effects. *Proc. Natl. Acad. Sci. USA* **2021**, *118*, e2013825118. [CrossRef]
83. Emergence of Gamma distributions in granular materials and packing models. *Phys. Rev.* **2008**, *77*, 021309 [CrossRef]
84. Del Pezzo, E.; Bianco, F.; Saccorotti, G. Seismic source dynamics at Vesuvius volcano, Italy. *J. Volcanol. Geotherm. Res.* **2004**, *133*, 23–39. [CrossRef]
85. Bachura, M.; Fischer, T.; Doubravová, J.; Horálek, J. From earthquake swarm to a main shock–aftershocks: The 2018 activity in West Bohemia/Vogtland. *Geophys. J. Int.* **2020**, *224*, 1835–1848. [CrossRef]
86. Uchide, T.; Imanishi, K. Underestimation of microearthquake size by the magnitude scale of the Japan Meteorological Agency: Influence on earthquake statistics. *J. Geophys. Res.* **2018**, *123*, 606–620. [CrossRef]
87. Iannaccone, G.; Alessio, G.; Borriello, G.; Cusano, P.; Petrosino, S.; Ricciolino, P.; Talarico, G.; Torello, V. Characteristics of the seismicity of Vesuius and Campi Flegrei during the year 2000. *Ann. Geofis.* **2001**, *44*, 1075–1091.
88. Giuidicepietro, F.; De Cesare, W.; Martini, M.; Meglio, V. Il sistema sismometrico modulare integrato (SISMI). *Open File Rep.* **2000**, *6*, 1–25.
89. Del Pezzo, E.; Petrosino, S. A local-magnitude scale for Mt. Vesuvius from synthetic Wood-Anderson seismograms. *J. Seismol.* **2001**, *5*, 207–215. [CrossRef]
90. Neunhöfer, H.; Hemmann, A. Earthquake swarms in the Vogtland/Western Bohemia region: Spatial distribution and magnitude–frequency distribution as an indication of the genesis of swarms? *J. Geodyn.* **2005**, *39*, 361–385. [CrossRef]
91. Dorbath, L.; Cuenot, N.; Genter, A.; Frogneux, M. Seismic response of the fractured and faulted granite of Soultz-sous-Forêts (France) to 5 km deep massive water injections. *Geophys. J. Int.* **2009**, *177*, 653–675. [CrossRef]
92. Farrell, J.; Husen, S.; Smith, R.B. Earthquake swarm and b-value characterization of the Yellowstone volcano-tectonic system. *J. Volcanol. Geotherm. Res.* **2009**, *188*, 260–276. [CrossRef]